plasma

MDPI

Article

Extracting Physical Information from the Voigt Profile Using the Lambert *W* Function

Jean-Christophe Pain [1,2]

[1] CEA, DAM, DIF, F-91297 Arpajon, France; jean-christophe.pain@cea.fr
[2] Université Paris-Saclay, CEA, Laboratoire Matière en Conditions Extrêmes, F-91680 Bruyères-le-Châtel, France

Abstract: Spectral line shapes are a key ingredient of hot-plasma opacity calculations. Since resorting to elaborate line-shape models remains prohibitive for intensive opacity calculations involving ions in different excitation states, with *L*, *M*, etc., shells are populated, and Voigt profiles often represent a reliable alternative. The corresponding profiles result from the convolution of a Gaussian function (for Doppler and sometimes ionic Stark broadening) and a Lorentzian function, for radiative decay (sometimes referred to as "natural" width) and electron-impact broadening. However, their far-wing behavior is incorrect, which can lead to an overestimation of the opacity. The main goal of the present work was to determine the energy (or frequency) at which the Lorentz wings of a Voigt profile intersect with the underlying Gaussian part of the profile. It turns out that such an energy cut-off, which provides us information about the dominant line-broadening process in a given energy range, can be expressed in terms of the Lambert *W* function, which finds many applications in physics. We also review a number of representations of the Voigt profile, with an emphasis on the pseudo-Voigt decomposition, which lends itself particularly well to cut-off determination.

Keywords: dense plasma; atomic spectroscopy; spectral line shapes; Voigt profile; Lambert's function

Citation: Pain, J.-C. Extracting Physical Information from the Voigt Profile Using the Lambert *W* Function. *Plasma* **2024**, *7*, 427–445. https://doi.org/10.3390/plasma7020023

Academic Editor: Andrey Starikovskiy

Received: 29 March 2024
Revised: 14 May 2024
Accepted: 24 May 2024
Published: 27 May 2024

1. Introduction

The main recent improvements of calculations of photon absorption by plasma come mainly from a better treatment of the photo-excitation (bound-bound) spectrum, either with DLA (Detailed Line Accounting) or statistical methods. Theoretical photon absorption exhibits a strong dependence on spectral line-shape models. Unfortunately, it is impossible with the present codes to implement elaborate line-broadening mechanisms [1–4]. For this reason, the opacity codes employ simpler approximations. The usual procedure consists of performing the convolution of a Gaussian function, due to Doppler broadening, and a Lorentzian function, due to the natural lifetime plus electron impact widths. The absorption coefficient of a line (frequency ν_0 and strength S) at the photon frequency ν reads as follows:

$$\kappa_\nu(x,y) = \frac{S\sqrt{\ln 2}}{\sqrt{\pi}\gamma_G} K(x,y), \tag{1}$$

where $x = (\nu - \nu_0)\sqrt{\ln 2}/\gamma_G$, $y = \gamma_L\sqrt{\ln 2}/\gamma_G$ (γ_L and γ_G are the HWHM (half with at half maximum) values of the Lorentzian and Gaussian profiles, respectively), and

$$K(x,y) = \frac{y}{\pi}\int_{-\infty}^{\infty} \frac{e^{-t^2}}{(x-t)^2+y^2} dt. \tag{2}$$

The latter function is the so-called Voigt profile [5] and can be expressed as follows:

$$K(x,y) = \Re[w_1(z)], \tag{3}$$

where $\Re(z)$ denotes the real part of complex number z, and

$$\begin{aligned} w_1(z) &= e^{-z^2}\left(1+\frac{2i}{\sqrt{\pi}}\int_0^z e^{t^2}dt\right), \\ &= e^{-z^2}[1+\mathrm{erf}(iz)] = e^{-z^2}[1-\mathrm{erf}(-iz)] = e^{-z^2}\mathrm{erfc}(-iz), \end{aligned} \tag{4}$$

is sometimes called the Faddeyeva–Terent'ev [6–8] function or complex error function [9]. Equation (4) is proven in Appendix A. Several methods have been proposed in order to calculate the Voigt function [10–26]. It can, for instance, be expressed as a series of confluent hypergeometric functions [27,28]. A good review of different families of methods was given by Schreier [29]. Some interesting relationships (particularly from the historical point of view) are recalled in Appendix B.

In hot plasma, near the line center, the Voigt profile is usually the convolution of a relatively broad Gaussian profile with a narrow Lorentzian profile, and so, it resembles the Gaussian profile. That is, at $\nu \approx \nu_0$, we can replace e^{-t^2} in the integrand of the right-hand side of Equation (2) with e^{-x^2} and integrate over the new variable $u = x - t$ so that

$$K(x,y) \approx \left(\frac{y}{\pi}\right) e^{-x^2}\int_{-\infty}^{\infty}\frac{du}{u^2+y^2} \approx e^{-x^2}. \tag{5}$$

The wings of the profile are governed by the Lorentzian function, which has much broader wings than the Gaussian function. This means that it is far away from the Doppler core where $x \gg 1$, so that (with $y \ll 1$, i.e., the full width at half maximum (FWHM) of the natural/collision broadening is much smaller than the FWHM of the Doppler broadening) replacing $x - t$ with x in the integrand of the right-hand side of Equation (2) results in the following:

$$K(x,y) \approx \frac{y}{\pi}\int_{-\infty}^{\infty}\frac{e^{-t^2}}{x^2}dt = \frac{y}{\pi}\frac{\sqrt{\pi}}{x^2} = \frac{y}{\sqrt{\pi}x^2}. \tag{6}$$

Due to the ionic microfield distribution, the quasi-static approximation applies for photon frequencies larger than the Weiskopf frequency and should decrease roughly as $\nu^{-5/2}$. The Voigt profile has incorrect far-wing behavior and, therefore, can significantly overestimate the photon absorption. The goal of the present work was to determine the energy at which the Lorentz wings of a Voigt profile intersect with the underlying Gaussian part of the profile. It was found that such a value can be expressed with the Lambert function.

In Section 2, we provide a non-exhaustive list of different families of representations of the Voigt function. The widely used pseudo-Voigt approximation is introduced in Section 3. The "competition" between the Lorentzian and Gaussian functions in the Voigt profile is studied in Section 4 with the help of the Lambert W function, and issues related to the far-wing behavior of the profile are discussed in Section 5.

2. Representations of the Voigt Function: A Non-Exhaustive Mini-Review

In this section, we provide a non-exhaustive list of representations of the Voigt function. A long time ago, Fettis [30] and Katriel [31] obtained the following (see also Ref. [32]):

$$\begin{aligned} K(x,y) = &\exp(y^2-x^2)\cos(2xy) - \frac{1}{\sqrt{\pi}}\left\{(y+ix)\,{}_1F_1\left[1;\frac{3}{2};(y+ix)^2\right]\right. \\ &\left.+(y-ix)\,{}_1F_1\left[1;\frac{3}{2};(y-ix)^2\right]\right\}, \end{aligned} \tag{7}$$

where ${}_1F_1$ is the Kummer confluent hypergeometric function, and Yang proposed the following representations [33]:

$$K(x,y) = \frac{1}{2\sqrt{\pi}}\Big\{(y-ix)^{-1/2}\exp\Big[(y-ix)^2/2\Big]W_{-1/4,-1/4}\Big[(y-ix)^2\Big] + (y+ix)^{-1/2}\exp\Big[(y+ix)^2/2\Big]W_{-1/4,-1/4}\Big[(y+ix)^2\Big]\Big\}, \quad (8)$$

where W represents the Whitaker function, and

$$K(x,y) = \frac{1}{2}\Big\{\exp\Big[(y-ix)^2\Big]\,\mathrm{erfc}(y-ix) + \exp\Big[(y+ix)^2\Big]\,\mathrm{erfc}(y+ix)\Big\} \quad (9)$$

and

$$K(x,y) = \frac{1}{\sqrt{2\pi}}\Big\{\exp\Big[(y-ix)^2/2\Big]D_{-1}\Big[\sqrt{2}(y-ix)\Big] + \exp\Big[(y+ix)^2/2\Big]D_{-1}\Big[\sqrt{2}(y+ix)\Big]\Big\}, \quad (10)$$

where

$$D_{-1}(z) = e^{-z^2}\int_0^z e^{t^2}dt. \quad (11)$$

More recently, Di Rocco derived an expression as an infinite sum over Kummer confluent hypergeometric functions ${}_1F_1$ [34]:

$$K(x,y) = \sum_{n=0}^{\infty}(-1)^n\left\{\frac{1}{\Gamma(n+1)}\,{}_1F_1\left(n+\frac{1}{2},\frac{1}{2};y^2\right) - \frac{2y}{\Gamma\left(n+\frac{1}{2}\right)}\,{}_1F_1\left(n+1,\frac{3}{2};y^2\right)\right\}, \quad (12)$$

while Zaghloul obtained [35]

$$\begin{aligned} K(x,y) &= [1-\mathrm{erf}(y)]\,\exp\Big[-x^2+y^2\Big]\cos(2xy) \\ &\quad + \frac{2}{\sqrt{\pi}}\int_0^x \exp(-x^2+\xi^2)\sin[2y(x-\xi)]d\xi \end{aligned} \quad (13)$$

and Limandri obtained [36]

$$\begin{aligned} K(x,y) &= \exp(-x^2+y^2)(\mathrm{erfc}(y)\cos(2xy)) \\ &\quad + \cos(2xy)\{\mathrm{erf}(y) - \Re[\mathrm{erf}(y+ix)]\} \\ &\quad + \sin(2xy)\,\Im[\mathrm{erf}(y+ix)]), \end{aligned} \quad (14)$$

where $\Im(z)$ represents the imaginary part of complex number z. As mentioned in Ref. [25], He and Zhang claimed to have obtained an exact expression of the Voigt profile that is proportional to the product of an exponential and a cosine function. However, Pagnini and Saxena [25] pointed out that such a representation assumes negative values, which is not correct. Such an issue was also commented on by Zaghloul [37]. Pagnini and Saxena also proposed to express the Voigt function in terms of Fox functions [38–40]:

$$H_{pq}^{mn}\left[z\,\middle|\,\begin{matrix}(a_1,A_1),\cdots,(a_p,A_p)\\(b_1,B_1),\cdots,(b_q,B_q)\end{matrix}\right] = \frac{1}{2\pi i}\int_{\mathscr{L}} h(s)z^s ds, \quad (15)$$

with

$$h(s) = \frac{\prod_{j=1}^{m}\Gamma\left(b_j - B_j s\right)\prod_{j=1}^{n}\Gamma\left(1-a_j+A_j s\right)}{\prod_{j=m+1}^{q}\Gamma\left(1-b_j+B_j s\right)\prod_{j=n+1}^{n}\Gamma\left(a_j - A_j s\right)}. \quad (16)$$

The integration path $\mathscr{L}$ is the contour that separates the points $s = (b_j+k)/B_j$, $j = 1,\cdots,m$ and $k = 0,1,\ldots$, which are the poles of $\Gamma(b_j - B_j s)$ (still for $j = 1,\cdots,m$) from the points $s = (a_j - k - 1)/A_j$, $j = 1,\cdots,n$, which are the poles of $\Gamma(1-a_j+A_j s)$ ($j = 1,\cdots,n$). The more common Meijer functions G_{pq}^{mn} are special cases of Fox functions for which $A_j = B_k = 1$, $j = 1,\cdots,p$, $k = 1,\cdots,q$, i.e.,

$$H_{pq}^{mn}\left[z\,\middle|\,\begin{matrix}(a_1,1),\cdots,(a_p,1)\\(b_1,1),\cdots,(b_q,1)\end{matrix}\right]=\mathrm{G}_{pq}^{mn}\left[z\,\middle|\,\begin{matrix}a_1,\cdots,a_p\\b_1,\cdots,b_q\end{matrix}\right] \tag{17}$$

and the corresponding Voigt profile reads

$$V(x)=\frac{1}{2\pi\omega_G}\left\{H_{11}^{11}\left[\frac{2}{\omega_G}(\omega_L+ix)\,\middle|\,\begin{matrix}(\frac{1}{2},\frac{1}{2})\\(0,1)\end{matrix}\right]+H_{11}^{11}\left[\frac{2}{\omega_G}(\omega_L-ix)\,\middle|\,\begin{matrix}(\frac{1}{2},\frac{1}{2})\\(0,1)\end{matrix}\right]\right\} \tag{18}$$

or equivalently,

$$V(x)=\frac{1}{2\pi\omega_G}\left\{H_{11}^{11}\left[\frac{\omega_G}{2(\omega_L+ix)}\,\middle|\,\begin{matrix}(1,1)\\(\frac{1}{2},\frac{1}{2})\end{matrix}\right]+H_{11}^{11}\left[\frac{\omega_G}{2(\omega_L-ix)}\,\middle|\,\begin{matrix}(0,1)\\(\frac{1}{2},\frac{1}{2})\end{matrix}\right]\right\}. \tag{19}$$

Setting

$$Z=\frac{2(\omega_L+ix)}{\omega_G}, \tag{20}$$

and expressing the Voigt profile in the form

$$V(x)=\int_{-\infty}^{\infty}L(x-\xi)G(\xi)d\xi \tag{21}$$

with the Gaussian function

$$G(x)=\frac{1}{\sqrt{\pi}\omega_G}\exp\left[-\left(\frac{x}{\omega_G}\right)^2\right] \tag{22}$$

and the Lorentzian function

$$L(x)=\frac{\omega_L}{\pi}\frac{1}{x^2+\omega_L^2}, \tag{23}$$

yield

$$V(x)=\frac{\omega_L}{\omega_G\pi^{3/2}}\int_{-\infty}^{\infty}\frac{\exp\left[-\left(\frac{\xi}{\omega_G}\right)^2\right]}{(x-\xi)^2+\omega_L^2}d\xi, \tag{24}$$

and finally,

$$V(x)=\frac{1}{2\pi^{3/2}\omega_G}\left\{\mathrm{G}_{12}^{21}\left[\frac{Z^2}{4}\,\middle|\,\begin{matrix}\frac{1}{2}\\(0,\frac{1}{2})\end{matrix}\right]+\mathrm{G}_{12}^{21}\left[\frac{\bar{Z}^2}{4}\,\middle|\,\begin{matrix}\frac{1}{2}\\(0,\frac{1}{2})\end{matrix}\right]\right\}. \tag{25}$$

Throughout the manuscript, and especially in the present section, since we review different published approximations, we decided, in order to avoid the introduction of typographical errors, to keep the notations of the corresponding authors. This is also justified because the choices made by these authors are often of interest (in terms of simplicity, physical context, etc.). However, in every case, we try to indicate the correspondence between the different quantities. For instance, the parameters involved in $K(x,y)$ in Equation (2) and in $V(x)$ from Equation (21) are related by

$$\omega_G=\frac{\gamma_G}{\sqrt{\ln 2}};\quad \omega_L=\gamma_L. \tag{26}$$

Figure 1 represents the Gaussian, Lorentzian, and Voigt functions. The Gaussian is such that $2\sigma^2=1$; and the Lorentzian, such that $\gamma=1$ (see Equations (28) and (29), respectively).

Finally, within a different approach, we believe that the Tepper-García function is worth mentioning. It consists of a combination of an exponential function and rational functions that approximate the line-broadening function $H(a,u)$ over a wide range of its parameters [41] (see Appendix C).

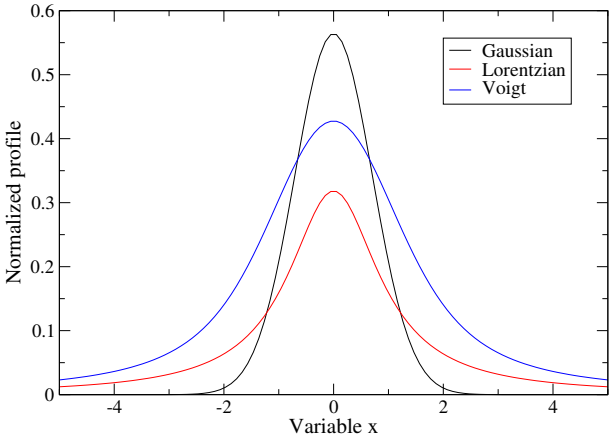

Figure 1. Gaussian, Lorentzian, and Voigt profiles. The Gaussian is such that $2\sigma^2 = 1$; and the Lorentzian, such that $\gamma = 1$ (see Equations (28) and (29), respectively).

3. The Pseudo-Voigt Function

3.1. Main Principle

The pseudo-Voigt profile (or pseudo-Voigt function) is an approximation of the Voigt profile $V(x)$ using a linear combination of a Gaussian $G(x)$ and a Lorentzian $L(x)$ function instead of their convolution. The pseudo-Voigt function is often used for calculations of experimental spectral line shapes [42,43]. The mathematical definition of the normalized pseudo-Voigt profile is given by

$$V_p(x, f_V) = \eta\, L(x, \gamma_L) + (1 - \eta)\, G(x, \gamma_G) \tag{27}$$

where

$$G(x; \sigma) \equiv \frac{e^{-x^2/(2\sigma^2)}}{\sigma\sqrt{2\pi}}, \tag{28}$$

and $L(x; \gamma)$ is the centered Lorentzian profile:

$$L(x; \gamma) \equiv \frac{\gamma}{\pi(x^2 + \gamma^2)} \tag{29}$$

with $0 < \eta < 1$, η being a function of the HWHM parameters of the Voigt, Lorentzian, and Gaussian FWHM parameters (respectively, γ_V, γ_L, and γ_G). The HWHM of the Gaussian profile is

$$\gamma_G = \sigma\sqrt{2\ln(2)}, \tag{30}$$

and the HWHM of the Lorentzian profile is

$$\gamma_L = \gamma. \tag{31}$$

There are several possible choices for the η parameter [44–47]. It turns out that a simple formula, accurate to 1%, is as follows [48,49]:

$$\eta = 1.36603\left(\frac{\gamma_L}{\gamma_V}\right) - 0.47719\left(\frac{\gamma_L}{\gamma_V}\right)^2 + 0.11116\left(\frac{\gamma_L}{\gamma_V}\right)^3, \tag{32}$$

where η is a function of the Lorentz (γ_L), Gaussian (γ_G), and total (γ_V) HWHM parameters, with the latter being described by

$$\gamma_V = \left[\gamma_G^5 + 2.69269\,\gamma_G^4\gamma_L + 2.42843\,\gamma_G^3\gamma_L^2 + 4.47163\,\gamma_G^2\gamma_L^3 + 0.07842\,\gamma_G\gamma_L^4 + \gamma_L^5\right]^{1/5}. \tag{33}$$

An approximate relation (accurate to within about 1.2%) between the widths of the Voigt, Gaussian, and Lorentzian profiles is as follows[50]:

$$\gamma_V \approx \frac{\gamma_L}{2} + \sqrt{\frac{\gamma_L^2}{4} + \gamma_G^2}. \tag{34}$$

By construction, this expression is exact for a pure Gaussian or Lorentzian. A better approximation with an accuracy of 0.02% was given by Olivero et al. [51] (originally found by Kielkopf [52]):

$$\gamma_V \approx 0.5346\,\gamma_L + \sqrt{0.2166\,\gamma_L^2 + \gamma_G^2}. \tag{35}$$

Expression (35) is also exact for a pure Gaussian or Lorentzian.

3.2. Matveev's Analytical Approximation of the Voigt Profile and the "Equivalent" Width of the Voigt Profile

Another approximation, resulting in the summation of a Gaussian and a Lorentzian, was proposed by Matveev [12]:

$$\kappa_\nu(\eta, \xi) = \frac{S}{\sqrt{\pi}\gamma_V}\left(\sqrt{\ln 2}\,(1-\xi)\,e^{-\eta^2 \ln 2} + \frac{\xi}{\sqrt{\pi}}\frac{1}{1+\eta^2}\right), \tag{36}$$

where $\xi = \gamma_L/\gamma_V$, $\eta = (\nu - \nu_0)/\gamma_V$, and γ_V is the equivalent width [51] of the Voigt profile, which can be calculated by

$$\gamma_V = \frac{1}{2}\left(\gamma_L + \sqrt{\gamma_L^2 + 4\gamma_G^2}\right) + 0.05\left(1 - \frac{2\gamma_L}{\gamma_L + \sqrt{\gamma_L^2 + 4\gamma_G^2}}\right). \tag{37}$$

The latter expression is exact in two limiting cases: $\xi = 0$ and $\xi = 1$ (pure Gaussian and Lorentzian). Note that the accuracy of Matveev's approximation was improved by Dobrichev [53].

3.3. Equivalent Width According to He and Zhang

Using a Fourier transform and Taylor series, He and Zhang [54,55] obtained

$$\gamma_V = \frac{\gamma_G}{\sqrt{1 + 8\pi^2(\ln 2)\left(\frac{\gamma_L}{\gamma_G}\right)^2}} \tag{38}$$

with

$$f(\nu - \nu_0) = \frac{f'y}{\pi}\int_{-\infty}^{\infty} \frac{e^{-t^2}}{y^2 + (x-t)^2}dt \tag{39}$$

with $y = \ln 2(\gamma_L/\gamma_G)$, $x = (\nu - \nu_0)\sqrt{\ln 2}/\gamma_G$, and $f' = \sqrt{\ln 2}/\gamma_G$, where γ_L and γ_G are the HWHM of the Lorentzian and Gaussian functions, respectively. Using the Fourier and inverse Fourier transforms, He and Zhang obtained an accurate Voigt profile as follows:

$$f(z) = \sqrt{\pi f'[\exp(4\pi y^2 - z^2)\cos(4\pi yz) + \exp(4\pi y^2 - x^2)\cos(4\pi yx)]} \tag{40}$$

with

$$z = \left(\frac{\nu + \nu_0}{\gamma_G}\right)\sqrt{\ln 2}. \tag{41}$$

They also provided a relationship between the HWHM of the Voigt profile and the HWHM of the Gaussian and Lorentzian profiles [56]:

$$\ln\left[\cos\left(\frac{4\pi(\ln 2)\gamma_L\gamma_V}{\gamma_G^2}\right)\right] = \frac{(\gamma_V^2-\gamma_G^2)}{\gamma_G^2}\ln 2 = \ln\left[2^{\frac{(\gamma_V^2-\gamma_G^2)}{\gamma_G^2}}\right]. \tag{42}$$

Using the expansions

$$\cos x = 1 - \frac{x^2}{2} + \frac{x^4}{4!} - \frac{x^6}{6!} + \cdots \tag{43}$$

as well as

$$2^x = 1 + x\ln 2 + \frac{x^2}{2}(\ln 2)^2 + \frac{x^3}{3!}(\ln 2)^3 + \cdots \tag{44}$$

we obtain the following, considering the first two terms only:

$$1 - \frac{16\pi^2(\ln 2)^2\gamma_L^2\gamma_V^2}{2\gamma_G^2} = 1 + \frac{(\gamma_V^2-\gamma_G^2)}{\gamma_G^2}\ln 2, \tag{45}$$

yielding

$$\left(\frac{\gamma_V}{\gamma_G}\right)^2 + 8\pi^2\ln 2\left(\frac{\gamma_L}{\gamma_G}\right)^2 = 1. \tag{46}$$

It is important to mention that Wang et al. presented a simple approximation scheme to describe the half width of the Voigt profile as a function of the relative contributions of the Gaussian and Lorentzian broadening [57]. The proposed approximation scheme is highly accurate and provides an accuracy better than 10^{-17} for arbitrary γ_L/γ_G ratios. In particular, the accuracy reaches an astonishing 10^{-34} (quadruple precision) in the domains $0 \leq \gamma_L/\gamma_G \leq 0.2371$ and $\gamma_L/\gamma_G \geq 33.8786$.

4. Competition between Lorentzian and Gaussian Wings

4.1. Mathematical Formalism

In Hui's algorithm [13], which computes the complex error function with rational approximation, the exponential decrease e^{-x^2} is not well described for vanishing y. In order to avoid that, it was suggested by Karp [58] to replace Hui's approximation for the real part of the complex error function with an *ansatz* for small y and $y/x^2 < 10^{-4}$. Using a Fourier transform expression [59,60],

$$K(x,y) = \frac{1}{\sqrt{\pi}}\int_0^\infty e^{-yu-\frac{u^2}{4}}\cos(xu)du \tag{47}$$

and, for $y \ll 1$, the first-order approximation $e^{-yu} \approx 1 - yu$, one finds that

$$\begin{aligned} K(x,y) &\approx \frac{1}{\sqrt{\pi}}\int_0^\infty e^{-\frac{u^2}{4}}\cos(xu)du - \frac{y}{\sqrt{\pi}}\int_0^\infty ue^{-\frac{u^2}{4}}\cos(xu)du \\ &= \frac{2}{\sqrt{\pi}}\int_0^\infty e^{-t^2}\cos(2xt)dt - \frac{2y}{\sqrt{\pi}}\int_0^\infty 2te^{-t^2}\cos(2xt)dt, \end{aligned} \tag{48}$$

where we have made a change of variables $t = u/2$. One now has

$$\frac{2}{\sqrt{\pi}}\int_0^\infty e^{-t^2}\cos(2xt)dt = e^{-x^2} \tag{49}$$

and

$$\begin{aligned} \int_0^\infty 2te^{-t^2}\cos(2xt)dt &= 1 - 2x\int_0^\infty e^{-t^2}\sin(2xt)dt \\ &= 1 - 2xe^{-x^2}\int_0^x e^{u^2}du \equiv 1 - 2xF(x), \end{aligned} \tag{50}$$

which leads to the following equation. Note that the two terms on the right-hand side of Equation (51) are the first two terms of an expansion (see Appendix D).

$$K(x,y) \approx e^{-x^2} - \frac{2y}{\sqrt{\pi}}[1 - 2xF(x)] \tag{51}$$

Then, using the asymptotic expansion

$$1 - 2xF(x) = -\left[\frac{1}{2x^2} + \frac{1.3}{(2x^2)^2} + \frac{1.3.5}{(2x^2)^3} + \frac{1.3.5.7}{(2x^2)^4} + \cdots\right] \tag{52}$$

truncated at the first order in x^2, one obtains the following [10,29,60]:

$$K(x,y) \approx e^{-x^2} + \frac{y}{\sqrt{\pi}\, x^2}. \tag{53}$$

The Voigt profile corresponds to the same parameters. Figure 2 displays the forms e^{-x^2}, $1/(\sqrt{\pi}x^2)$ (see Equation (53)), and the same Voigt profile as in Figure 1. Figure 3 shows the functions e^{-x^2}, $\gamma/(\sqrt{\pi}x^2)$ (see Equation (53)) with $\gamma = 0.2$, and the Voigt profile $K(x, 0.2)$ (see Equation (2)). Compared to in Figure 2, the shape of the Lorentzian is "sharper" and more concentrated near the origin. In this case, the Voigt profile is dominated by the Lorentzian close to the center of gravity, but also for higher values of x. The Lorentzian wings are recovered much farther away.

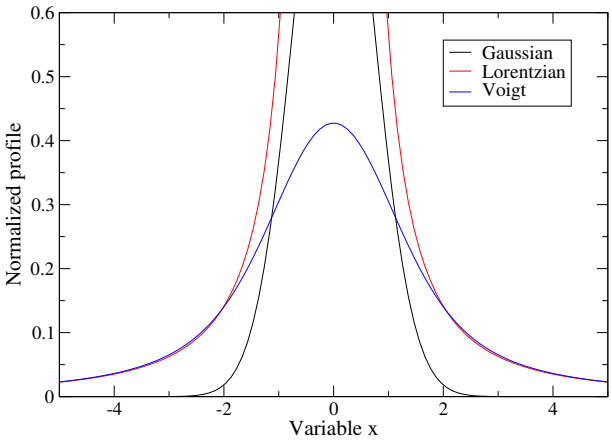

Figure 2. Functions e^{-x^2} (Gaussian), $1/\sqrt{\pi}/x^2$ (Lorentzian) (see Equation (53)), and the same Voigt profile shown in Figure 1.

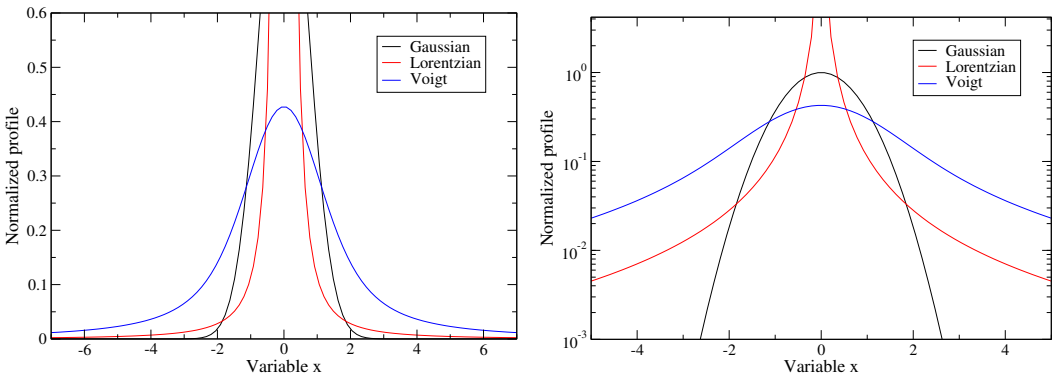

Figure 3. (**Left**): Functions e^{-x^2} and $\gamma/\sqrt{\pi}/x^2$ (see Equation (53)) with $\gamma = 0.2$ and the Voigt profile $K(x, 0.2)$ (see Equation (2)). (**Right**): The same functions but with a logarithmic scale for the y-axis.

One searches for the critical value x_c, for which the Lorentz wings intersect with the Gaussian, such that

$$e^{-x_c^2} = \frac{y}{\sqrt{\pi}\, x_c^2}. \tag{54}$$

which reads equivalently to

$$x_c^2\, e^{-x_c^2} = \frac{y}{\sqrt{\pi}}. \tag{55}$$

The solution of the latter equation can be written as

$$x_c = -\sqrt{W_{-1}\left(-\frac{y}{\sqrt{\pi}}\right)}, \tag{56}$$

where W_{-1} represents Lambert's function [61,62]. This function appears in various fields of physics, such as Wien's displacement law; the fringing fields of a capacitor, with the latter problem being representative of some problems solved using conformal transformations; the resolution of the Schrödinger equation in a generic radial grid; etc. [63–68], but also in mathematics, for instance, in the study of prime numbers [69]. The function (see Figure 4), named after Lambert, who was faced with a related problem [61], was described by Euler [70].

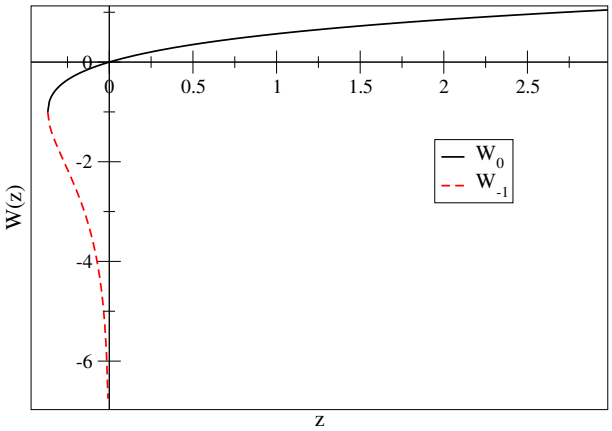

Figure 4. Representation of the two branches of the Lambert function.

For each integer k there is one branch, denoted by $W_k(z)$, which is a complex-valued function of one complex argument. W_0 is known as the principal branch. When dealing with real numbers only, the two branches W_0 and W_{-1} suffice: the equation $ye^y = x$ can be solved for y only if $x \geq -1/e$. We obtain $y = W_0(x)$ if $x \geq 0$, and the two values $y = W_0(x)$ and $y = W_{-1}(x)$, if $-1/e \leq x < 0$.

4.2. Application in the Case of the Pseudo-Voigt Function of Matveev

Using Matveev's pseudo-Voigt function [12] (see Equation (36)), the value of parameter η for which the Gaussian and the Lorentzian intersect with each other is obtained by solving

$$(1-\xi)\, e^{-\eta^2 \ln 2} = \frac{\xi}{\sqrt{\pi \ln 2}} \frac{1}{1+\eta^2}, \tag{57}$$

which can be written equivalently as

$$-(1+\eta^2)(\ln 2)\, e^{-(1+\eta^2)\ln 2} = -\frac{1}{2}\sqrt{\frac{\ln 2}{\pi}}\frac{\xi}{1-\xi}. \tag{58}$$

The solution of the latter equation is

$$\eta = \sqrt{-1 - \frac{1}{\ln 2} W_{-1}\left[-\frac{1}{2}\sqrt{\frac{\ln 2}{\pi}}\frac{\xi}{1-\xi}\right]}. \tag{59}$$

4.3. Calculation of the Lambert W Function

Besides the theoretical advantages of providing an adequate analytical solution to our problem, another benefit of the Lambert W function is the availability of libraries in computer algebra systems, which allows for a convenient way to obtain values, expansions, plots, etc. We have the following expansion for the Lambert function W [71–73]:

$$W(x) = \ln x - \ln\ln x + \sum_{k=0}^{\infty}\sum_{m=1}^{\infty} c_{km}\frac{(\ln\ln x)^m}{(\ln x)^{k+m}} \tag{60}$$

where

$$c_{km} = \frac{(-1)^k}{m!} S[k+m, k+1], \tag{61}$$

with $S[k+m, k+1]$ being a Stirling number of the first kind [74,75], for which an explicit expression was provided by Karanicoloff [76]. Stirling numbers can be obtained with recursion relations. We suggest using Equation (60) truncated at the fourth order:

$$\begin{aligned} W(x) &= \ln x - \ln\ln x + \frac{\ln\ln x}{\ln x} + \frac{\ln\ln x(\ln\ln x - 2)}{2(\ln x)^2} \\ &+ \frac{\ln\ln x(2(\ln\ln x)^2 - 9\ln\ln x + 6)}{6\ln^3 x} + O\left[\left(\frac{\ln\ln x}{\ln x}\right)^5\right]. \end{aligned} \tag{62}$$

The Lambert function satisfies many interesting properties. For instance, its derivative can be in the form

$$W'(x) = \frac{W(x)}{x[1+W(x)]} \tag{63}$$

and, more generally ($n \geq 1$),

$$\frac{d^n W(e^x)}{dx^n} = \frac{q_n(W(e^x))}{[1+W(e^x)]^{2n-1}} \tag{64}$$

where

$$q_n(w) = \sum_{k=0}^{n-1}(-1)^k \left\langle\!\left\langle {n-1 \atop k} \right\rangle\!\right\rangle w^{k+1}, \tag{65}$$

where $\left\langle\!\left\langle {a \atop b} \right\rangle\!\right\rangle$ represents second-order Eulerian numbers [77]. The anti-derivative of the Lambert W function reads

$$\int W(x)dx = x\left[W(x) - 1 + \frac{1}{W(x)}\right] \tag{66}$$

and one has

$$W(x) + W(y) = W\left(xy\left(\frac{1}{W(x)} + \frac{1}{W(y)}\right)\right). \tag{67}$$

5. Remarks on the Far Wings of the Voigt Profile

5.1. The Cut-Off of Iglesias et al.

It is well known by spectroscopists that the Voigt profile has incorrect far wing behavior and, therefore, can significantly overestimate the photon absorption. Iglesias et al. [78] proposed an extension of the Voigt profile that incorporates a far wing cut-off remaining computationally tractable. The second-order line width from electron collisions for a transition from level a to level b is proportional to the quantity $G_{ab}(\omega)$ [79–82] satisfying,

under the assumptions of a Debye plasma and the dipole approximation for the electron-radiator interaction with minimum impact parameter cut-off q_{ab}^{-1}, the limits

$$G_{ab}(\omega \to 0) = \frac{1}{2}\left\{\ln\left(1+\lambda_D^2 q_{ab}^2\right) - \frac{\lambda_D^2 q_{ab}^2}{1+\lambda_D^2 q_{ab}^2}\right\} \tag{68}$$

and

$$G_{ab}(\omega \to \infty) = G_{ab}^{\infty} = \frac{1}{2}E_1\left[X_{ab}^2\right] \to \frac{e^{-X_{ab}^2}}{2X_{ab}^2} \quad \text{when} \quad X_{ab} \to \infty \tag{69}$$

with

$$X_{ab}^2 = \frac{m_e}{2q_{ab}^2 T}(\omega + |\omega_a - \omega_b|)^2 \tag{70}$$

and the exponential integral

$$E_1(x) = \int_x^{\infty} \frac{e^{-t}}{t} dt. \tag{71}$$

The quantity λ_D represents the electron Debye length, defined as $\lambda_D^2 = T/(4\pi e^2 n_e)$, where n_e is the electron number density.

$$I_1(\omega) = Re[\mathscr{W}(\omega + ia, \omega)] \tag{72}$$

where $\mathscr{W}$ is the truncated error function (note that there is a typographical error in Equation (4.1.3) of Ref. [78]; $z - \omega$ should be replaced with $t - z$):

$$\mathscr{W}(z, \Omega) = \frac{1}{i\pi}\int_{\omega-\Omega}^{\omega+\Omega} dt \frac{e^{-t^2}}{t-z} \tag{73}$$

which can be evaluated with the sampling theorem [17]

$$\begin{aligned}\mathscr{W}(z,\Omega) \quad = \quad & \frac{h}{\pi^2}\Im\sum_{n=-N}^{N}\frac{e^{-t_n^2}}{z-t_n}\left\{\mathrm{Si}\left[\frac{\pi}{h}(\omega - t_n - \Omega)\right] - \mathrm{Si}\left[\frac{\pi}{h}(\omega + t_n + \Omega)\right]\right. \\ & + \left\{\mathrm{Ci}\left[\frac{\pi}{h}(\Omega - i\,a)\right] - \mathrm{Ci}\left[\frac{\pi}{h}(-\Omega - i\,a)\right]\sin\left[\frac{\pi}{h}(z-t_n)\right]\right\} \\ & \left. + \left\{\mathrm{Si}\left[\frac{\pi}{h}(\Omega + i\,a)\right] - \mathrm{Si}\left[\frac{\pi}{h}(-\Omega - i\,a)\right]\cos\left[\frac{\pi}{h}(z-t_n)\right]\right\}\right\},\end{aligned} \tag{74}$$

where $\mathrm{Si}(z)$ represents the sine integral

$$\mathrm{Si}(z) = \int_0^z \frac{\sin t}{t} dt \tag{75}$$

and $\mathrm{Ci}(z)$ represents cosine integral

$$\mathrm{Ci}(z) = -\int_0^z \frac{\cos t}{t} dt. \tag{76}$$

The decay parameter τ_{ab} is given by

$$\tau_{ab}^2 = \frac{m}{2q_{ab}^2 T} \tag{77}$$

and Ω is obtained solving

$$\Omega = \frac{\sqrt{y}}{\tau_{ab}} + |\omega_b - \omega_a| \tag{78}$$

obtained as the solution of

$$G_{ab}(0) = G_{ab}^{\infty}(\omega = \Omega) \tag{79}$$

and y is the solution of

$$y\, e^{y} = \frac{1}{2G_{ab}(0)}, \tag{80}$$

i.e.,

$$y = W\left(\frac{1}{2G_{ab}(0)}\right), \tag{81}$$

where W is the Lambert function.

5.2. Continued-Fraction Representation

The continued fraction for a function that has finite power moments of any order can be written in terms of the Laplace transform

$$\mathscr{F}(\omega) = \frac{1}{\pi}\Re\Big\{\mathscr{F}^{\mathrm{Lap}}(s = -i\omega)\Big\}. \tag{82}$$

For an even function, $\mathscr{F}(\omega) = \mathscr{F}(-\omega)$, the Laplace transform can be written as

$$\mathscr{F}^{\mathrm{Lap}}(s) = \frac{\mu_0}{s} - \frac{\mu_2}{s^3} + \frac{\mu_4}{s^5} + \cdots = \cfrac{b_0}{s + \cfrac{b_1}{s + \cfrac{b_2}{s + \cdots}}} \tag{83}$$

The continued fraction coefficients b_j are given in terms of the moments

$$\mu_{2n} = 2\int_0^\infty \omega^{2n}\mathscr{F}(\omega)d\omega \tag{84}$$

by a recursive relation [83,84]. The continued fraction representation can be expressed in the form

$$p(\omega) = \frac{1}{\pi}\Re\left\{\frac{1}{s + b_1\psi_1(s)}\right\}\Big|_{s=-i\omega} \tag{85}$$

with

$$\psi_n(s) = \frac{1}{s + b_{n+1}\psi_{n+1}(s)} \tag{86}$$

Inaccuracies can occur without an approximate expression for the termination function, $\psi_N(s)$. Unfortunately, the recursion relation for the b_n is numerically unstable, due to the emphasis of the power moments on larger frequencies. Appropriately chosen polynomials, rather than power moments, yield more stable formulas [85]:

$$\pi_{2n} = \frac{1}{(2\lambda)^{2n}}\int_{-\infty}^{\infty} d\omega H_{2n}(\lambda\omega)I_1(\omega) = (2n)!\sum_{k=0}^{n}\frac{\mu_{2k}}{(2k)!}\left\{\frac{\lambda^2-1}{4\lambda^2}\right\}^{n-k} \tag{87}$$

5.3. The Pearson Distribution: An Interesting Alternative?

In order to overcome the inadequacies of the Lorentzian, Gaussian, and Voigt functions, an alternative profile function, the Pearson VII function, is often used for peak fitting in, for example, X-ray diffraction [86]. The Pearson VII function is

$$I_P(\lambda) = I_0\left[1 + \left\{\frac{2(\lambda-\lambda_0)\sqrt{2^{1/M}-1}}{\Delta_P}\right\}^2\right]^{-M}, \tag{88}$$

where Δ_P is the FWHM, and M is known as the Pearson parameter. When M is equal to one, the distribution is identical to a Lorentzian, while as M becomes large, the distribution tends to a Gaussian. It is very much less computationally intensive than the Voigt function as it does not require numerical integration. To our knowledge, the Pearson VII distribution

has not been used in the analysis of plasma spectra. This is probably because there is no direct relationship between the plasma properties and the Pearson VII fit parameters, Δ_P and M [87], whereas the widths of the Lorentzian and Gaussian distributions, which can be extracted from fits to the Voigt function, can readily be related to the properties of the plasma.

6. Conclusions and Future Plans

Hot-plasma opacity calculations are sensitive to spectral line shapes. Since elaborate line-shape codes can hardly be tractable for intensive opacity calculations involving billions of lines of multi-charged ions in many different excitation states, Voigt profiles are often used. However, their far-wing behavior, which can lead to an overestimation of the opacity, is a persistent issue of opacity calculations. The main goal of the present work was to show that the variable (energy, frequency, etc.) at which the Lorentz wings of a Voigt profile intersect with the underlying Gaussian part of the profile involves the Lambert W function, giving the solution x of an equation of the kind $x\,e^x = b$. Such a quantity is important, in the general case, to know the physical broadening mechanisms that are dominating in a given energy range of the profile, but it becomes particularly interesting in the framework of "pseudo-Voigt" approximations of the Voigt profile, consisting of representing the latter as a sum of a Gaussian and a Lorentzian function, with appropriate weights. We took advantage of the opportunity to review a number of representations of the Voigt profile and to point out their weaknesses, in particular, as terms of the far wings. The literature about the Voigt profile is very abundant, and we decided to choose some specific representations, involving special functions such as the hypergeometric ${}_1F_1$ of Fox functions, which, in our opinion, have not been completely exploited and may lead to the derivation of new useful approximations. It is important to attach importance to different formulations, because each of them has its own advantages. For instance, the pseudo-Voigt function may be considered rather limited if one is interested in a high numerical accuracy, but it remains very practical for the interpretation of atomic or molecular spectra, or in order to determine the abscissa at which the Gaussian and the Lorentzian intersect with each other. The high number of available relations for the hypergeometric functions should also benefit the computation of the Voigt profile, either in order to derive recurrence relations or to investigate asymptotic properties. Finally, it is important to keep in mind that properly accounting for the Stark effect requires the convolution of the Voigt profile with an electric-microfield distribution. It would be interesting to repeat the present study with a simple modeling of the latter, for instance, by resorting to the Holtsmark function, for which appropriate analytical formulations may be derived [88,89].

Funding: This research received no external funding.

Institutional Review Board Statement: Not applicable.

Informed Consent Statement: Not applicable.

Data Availability Statement: The data presented in this study are available upon request from the corresponding author. The data are not publicly available due to privacy and ethical restrictions.

Conflicts of Interest: The author declares no conflicts of interest.

Abbreviations

The following abbreviations are used in this manuscript:

DFT	Density Functional Theory;
FWHM	Full Width at Half Maximum;
HWHM	Half Width at Half Maximum.

Appendix A. Proof of Faddeyeva–Terent'ev Relation

Let us consider the following function:

$$w_2(z) = \frac{i}{\pi}\int_{-\infty}^{\infty}\frac{e^{-t^2}}{z-t}dt. \tag{A1}$$

We want to show that $w_1(z) = w_2(z)$. From the theorem of isolated zeros, we can prove the latter equality on the imaginary axis $z = iy$ with $y > 0$. In this case, one has

$$\begin{aligned} w_1(z) &= e^{y^2}[1+\mathrm{erf}(-y)] = e^{y^2}[1-\mathrm{erf}(y)] = e^{y^2}\mathrm{erfc}(y) \\ &= e^{y^2}\left(1+\frac{2}{\sqrt{\pi}}\int_0^{-y}e^{-t^2}dt\right) = e^{y^2}\left(1-\frac{2}{\sqrt{\pi}}\int_0^{y}e^{-t^2}dt\right). \end{aligned} \tag{A2}$$

On the other side, one has

$$w_2(z) = \frac{i}{\pi}\int_{-\infty}^{\infty}\frac{e^{-t^2}}{iy-t}dt = e^{y^2}\frac{2y}{\pi}\int_0^{\infty}\frac{e^{-(t^2+y^2)}}{t^2+y^2}dt. \tag{A3}$$

Setting

$$I(y) = \frac{y}{\pi}\int_0^{\infty}\frac{e^{-(t^2+y^2)}}{t^2+y^2}dt \tag{A4}$$

and

$$J(y) = \frac{1}{2} - \frac{1}{\sqrt{\pi}}\int_0^{y}e^{-t^2}dt, \tag{A5}$$

one now needs to prove that $I(y) = J(y)$. A change in variables $t = yv$ in I leads to

$$I(y) = \frac{1}{\pi}\int_0^{\infty}\frac{e^{-y^2(1+v^2)}}{1+v^2}dv. \tag{A6}$$

Taking the derivative with respect to y yields

$$I'(y) = \frac{dI}{dy} = -\frac{1}{\sqrt{\pi}}e^{-y^2}. \tag{A7}$$

Therefore, one has $I'(y) = J'(y)$. Therefore, since $\lim_{y\to+\infty} I(y) = \lim_{y\to+\infty} J(y) = 0$, one has $I(y) \equiv J(y) \quad \forall y$. It is now possible to write $w_1(z) \equiv w_2(z)$, or in taking the real part, $\Re[w_1(z)] = \Re[w_2(z)]$, $\forall z$. Therefore,

$$K(x,y) = \frac{y}{\pi}\int_{-\infty}^{\infty}\frac{e^{-t^2}}{(x-t)^2+y^2}dt) = \Re\left[e^{-z^2}\left(1+\frac{2i}{\sqrt{\pi}}\int_0^{z}e^{t^2}dt\right)\right]. \tag{A8}$$

Appendix B. Additional Useful Relations

Fried and Conte [90,91] proposed the continued fraction representation

$$\sqrt{\pi}\,w(z) = \frac{1}{z+}\,\frac{1/2}{z+}\,\frac{1}{z+}\,\frac{3/2}{z+}\cdots\frac{n/2}{z+}\cdots \tag{A9}$$

One also has the following (see Abrarov [24]):

$$K(x,y) = \frac{2}{\pi}\int_{-\infty}^{\infty} t\,e^{-t^2}\arctan\left(\frac{t-x}{y}\right)dt \tag{A10}$$

which helps in finding asymptotic behaviors. Finally, it is interesting to mention the remarkable approximation for the Dawson function $F(z)$ [92],

$$F(z) = e^{-z^2} \int_0^z e^{t^2} dt, \tag{A11}$$

due to Rybicki [17]:

$$F(z) = \lim_{h \to 0} \frac{1}{\sqrt{\pi}} \sum_{n\ odd} \frac{e^{-(z-nh)^2}}{n}. \tag{A12}$$

Appendix C. The Tepper-García Function

The Tepper-García function [41] is obtained from a truncated power series expansion of the exact line-broadening function. In its most computationally efficient form, the Tepper-García function can be expressed as

$$T(a,u) = R - \left(a/\sqrt{\pi}P\right) \left[R^2 \left(4P^2 + 7P + 4 + Q\right) - Q - 1\right] \tag{A13}$$

where $P \equiv u^2$, $Q \equiv 3/(2P)$, and $R \equiv e^{-P}$. Thus the line-broadening function can be viewed, as a first order, as a pure Gaussian function plus a correction factor that depends linearly on the microscopic properties of the absorbing medium (encoded in a); however, as a result of the early truncation in the series expansion, the error in the approximation is still of order a, i.e.,

$$H(a,u) \approx T(a,u) + \mathcal{O}(a). \tag{A14}$$

This approximation has a relative accuracy of $\epsilon \equiv \left|H(a,u) - T(a,u)\right| / H(a,u) \lesssim 10^{-4}$ over the full wavelength range of $H(a,u)$, $a \lesssim 10^{-4}$. In addition to its high accuracy, the function $T(a,u)$ is easy to implement and is computationally fast. It is widely used in the field of quasar absorption line analysis [41,93].

Appendix D. Expansion of the Voigt Function

Let us start from

$$H(a,v) = \frac{1}{\sqrt{\pi}} \int_0^\infty e^{-\left(ax + x^2/4\right)} \cos(vx) dx. \tag{A15}$$

If $a \ll 1$, we can perform the series expansion of the exponential e^{-ax}. This yields the following [94]:

$$H(a,v) = \sum_{n=0}^{\infty} a^n G_n(v) \tag{A16}$$

where

$$G_n(v) = \frac{(-1)^n}{\sqrt{\pi} n!} \int_0^\infty e^{-x^2/4} x^n \cos(vx) dx. \tag{A17}$$

The G_n functions have been tabulated by Harris [95]. Since one has

$$\int_{-\infty}^{\infty} e^{-y^2} \cos(xy) dy = \sqrt{\pi}\, e^{-x^2/4}, \tag{A18}$$

one obtains

$$G_0(v) = e^{-v^2} \tag{A19}$$

and after integrating $G_1(v)$ by parts, one has

$$G_1(v) = -\frac{2}{\sqrt{\pi}} \left[1 - v \int_0^\infty e^{-x^2/4} \sin(vx) dx\right]. \tag{A20}$$

Then, since

$$\int_0^\infty e^{-y^2} \sin(2vy) dy = e^{-v^2} \int_0^\infty e^{y^2} dy = F(v), \tag{A21}$$

one obtains

$$G_1(v) = \frac{2}{\sqrt{\pi}}[2vF(v) - 1]. \tag{A22}$$

Note that G_0 (Equation (A19)) and G_1 (Equation (A20)) are the first two terms of Equation (51). For the next terms, one can use

$$G_n(v) = -\frac{1}{n(n-1)}\frac{d^2 G_{n-2}(v)}{dv^2}, \tag{A23}$$

and one finds

$$G_2(v) = \left(1 - 2v^2\right) e^{-v^2}, \tag{A24}$$

$$G_3(v) = -\frac{2}{\sqrt{\pi}}\left[\frac{2}{3}\left(1 - v^2\right) - 2v\left(1 - \frac{2}{3}v^2\right) F(v)\right], \tag{A25}$$

and

$$G_4(v) = \left(\frac{1}{2} - 2v^2 + \frac{2}{3}v^4\right) e^{-v^2}. \tag{A26}$$

The contributions G_1, G_2, G_3, and G_4 (given by Equations (A22), (A24), (A25) and (A26), respectively) are displayed in Figure A1.

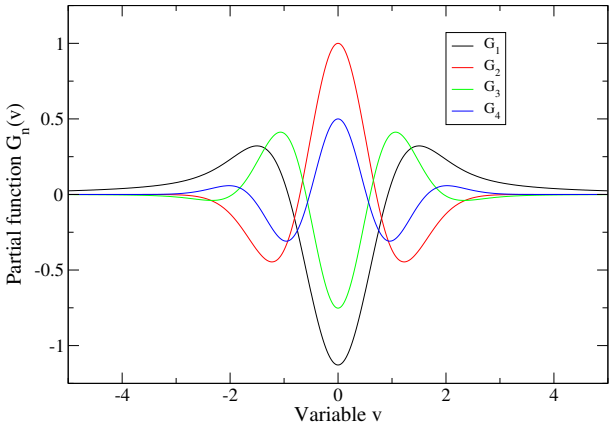

Figure A1. Contributions G_1, G_2, G_3, and G_4 (given by Equations (A22), (A24), (A25) and (A26), respectively) are the first terms in expansion (A16).

The functions of an even index G_{2p} take the form of a polynomial multiplied by e^{-v^2}, and the functions of an odd index $G_{2p}+1$ involve the Dawson function (see Equation (A11)).

References

1. Griem, H.R. *Spectral Line Broadening by Plasmas*; Academic Press: New York, NY, USA, 1974.
2. Calisti, A.; Khelfaoui, F.; Stamm, R.; Talin, B.; Lee, R.W. Model for the line shapes of complex ions in hot and dense plasmas. *Phys. Rev. A* **1990**, *42*, 5433–5440. [CrossRef] [PubMed]
3. Talin, B.; Calisti, A.; Godbert, L.; Stamm, R.; Lee, R.W.; Klein, L. Frequency-fluctuation model for line-shape calculations in plasma spectroscopy. *Phys. Rev. A* **1995**, *5*, 1918–1928. [CrossRef]
4. Stambulchik, E.; Maron, Y. Plasma line broadening and computer simulations: A mini-review. *High Energy Density Phys.* **2010**, *6*, 9–14. [CrossRef]
5. Voigt, W. Über das Gesetz der Intensitätsverteilung innerhalb der Linien eines Gasspektrums. *Munch. Sitzber Ak. Wiss. Math.-Phys. Kl.* **1912**, *42*, 603–620.
6. Faddeyeva, V.N.; Terent'ev, N.M. *Tables of Values of the Function* $w(z) = e^{-z^2}(1 + (2i/\sqrt{\pi})\int_0^z e^{-t^2}dt)$ *for Complex Argument*; Pergamon Press: New York, NY, USA, 1961.
7. Faddeyeva, V.N.; Terent'ev, N.M. *Tables of Values of Error Function for a Complex Argument*; Gostekhizdat: Moscow, Russia, 1954. (In Russian)
8. Zaghloul, M.R.; Ali, A.N. Algorithm 916: Computing the Faddeyeva and Voigt functions. *ACM Trans. Math. Softw.* **2011**, *38*, 1–22. [CrossRef]
9. Abramowitz, M.; Stegun, A. *Handbook of Mathematical Functions*; Dover: New York, NY, USA, 1970; p. 298.

10. Armstrong, B.H. Spectrum line profiles: The Voigt function. *J. Quant. Spectrosc. Radiat. Transf.* **1967**, *7*, 61–88. [CrossRef]
11. Avrett, E.H.; Loeser, R. *Formation of Line and Continuous Spectra*; Smithsonian Astrophysical Observatory: Cambridge, MA, USA, 1969; Volume 303.
12. Matveev, V.S. Approximate representation of absorption coefficient and equivalent widths of lines with Voigt profile. *J. Appl. Spectrosc.* **1972**, *16*, 168–172. [CrossRef]
13. Hui, A.K.; Armstrong, B.H.; Wray, A.A. Rapid computation of the Voigt and complex error functions. *J. Quant. Spectrosc. Radiat. Transf.* **1978**, *19*, 509–516. [CrossRef]
14. Matveev, V.S. Approximate representations of the refractive index of a medium in the region of a Voigt-profile absorption line. *J. Appl. Spectrosc.* **1981**, *35*, 1043–1046. [CrossRef]
15. Humlíček, J. Optimized computation of the voigt and complex probability functions. *J. Quant. Spectrosc. Radiat. Transf.* **1982**, *27*, 437–444.
16. Nikiforov, A.F.; Novikov, V.G.; Uvarov, V.B. *Special Functions of Mathematical Physics. A Unified Introduction with Applications*; Translated from the Russian; Birkhäuser Verlag: Basel, Switzerland, 1988.
17. Rybicki, G.B. Dawson's integral and the sampling theorem. *Comput. Phys.* **1989**, *3*, 85–87. [CrossRef]
18. Shippony, Z.; Read, W.G. A highly accurate Voigt function algorithm. *J. Quant. Spectrosc. Radiat. Transf.* **1993**, *50*, 635–646. [CrossRef]
19. Abousahl, S.; Gourma, M.; Bickel, M. Fast Fourier transform for Voigt profile: Comparison with some other algorithms. *Nucl. Instrum. Methods Phys. Res. Sect. A Accel. Spectrometers Detect. Assoc. Equip.* **1997**, *395*, 231–236. [CrossRef]
20. Wells, R.J. Rapid approximation to the Voigt/Faddeeva function and its derivatives. *J. Quant. Spectrosc. Radiat. Transf.* **1999**, *62*, 294–298. [CrossRef]
21. Asfaw, A. A fast method of modeling spectral lines. *J. Quant. Spectrosc. Radiat. Transf.* **2001**, *70*, 129–137. [CrossRef]
22. Leiweke, R.J. Comment on "A new procedure for obtaining the Voigt function dependent upon the complex error function". *J. Quant. Spectrosc. Radiat. Transf.* **2007**, *103*, 597–600. [CrossRef]
23. Letchworth, K.L.; Benner, D.C. Rapid and accurate calculation of the Voigt function. *J. Quant. Spectrosc. Radiat. Transf.* **2007**, *107*, 173–192. [CrossRef]
24. Abrarov, S.M.; Quine, B.M.; Jagpal, R.K. A simple interpolating algorithm for the rapid and accurate calculation of the Voigt function. *J. Quant. Spectrosc. Radiat. Transf.* **2009**, *110*, 376–383. [CrossRef]
25. Pagnini, G.; Saxena, R.K. On Mellin–Barnes integral representation of Voigt profile function. *Forum Berl. Math. Ges.* **2012**, *23*, 47–64.
26. Chib, S.; Belafhal, A. Simple analytical expression of the Voigt profile. *Quantum Rep.* **2022**, *4*, 36–46. [CrossRef]
27. Keshavamurthy, R.S. Voigt lineshape functions as a series of confluent hypergeometric functions. *J. Phys. A Math. Gen.* **1987**, *20*, L273–L278. [CrossRef]
28. Lebedev, N.N. *Special Functions and Their Applications*; Dover: New York, NY, USA, 1972; p. 258.
29. Schreier, F. The Voigt and complex error function: A comparison of computational methods. *J. Quant. Spectrosc. Radiat. Transf.* **1992**, *48*, 743–762. [CrossRef]
30. Fettis, H.E. Remarks on a note by H Exton. *J. Phys. A Math. Gen.* **1983**, *16*, 663–664. [CrossRef]
31. Katriel, J. A comment on the reducibility of the Voigt functions. *J. Phys. A Math. Gen.* **1982**, *15*, 709–710. [CrossRef]
32. Exton, H. On the reducibility of the Voigt functions. *J. Phys. A Math. Gen.* **1981**, *14*, L75–L77. [CrossRef]
33. Yang, S. A unification of the Voigt functions. *Int. J. Math. Educ. Sci. Technol.* **1994**, *25*, 845–851. [CrossRef]
34. Di Rocco, H.O.; Iriarte, D.I.; Pomarico, J. General expression for the Voigt function that is of so special interest for applied spectroscopy. *Appl. Spectrosc.* **2001**, *55*, 822–826. [CrossRef]
35. Zaghloul, M.R. On the calculation of the Voigt line profile: A single proper integral with a damped sine integrand. *Mon. Not. R. Astron. Soc.* **2007**, *375*, 1043–1048. [CrossRef]
36. Limandri, S.P.; Bonetto, R.D.; Di Rocco, H.O.; Trincavelli, J.C. Fast and accurate expression for the Voigt function. Application to the determination of uranium M linewidths. *Spectrochim. Acta Part B At. Spectrosc.* **2008**, *63*, 962–967. [CrossRef]
37. Zaghloul, M.R. On the falsity of a claimed exact analytic formula for the calculation of Voigt spectral line profile. *Spectrochim. Acta Part B At. Spectrosc.* **2007**, *63*, 820–821. [CrossRef]
38. Mathai, A.M.; Saxena, R.K. *The H-Function with Applications in Statistics and Other Disciplines*; Wiley Eastern Limited: New Delhi, India; Bangalore, India; Bombay, India, 1978.
39. Kilbas, A.A.; Saigo, M. *H-Transforms. Theory and Applications*; CRC Press LLC: Boca Raton, FL, USA, 2004.
40. Srivastava, H.M.; Gupta, K.C.; Goyal, S.P. *The H-Functions of One and Two Variables with Applications*; South Asian Publisher: New Delhi, India, 1982.
41. Tepper-García, T. Voigt profile fitting to quasar absorption lines: An analytic approximation to the Voigt-Hjerting function. *Mon. Not. R. Astron. Soc.* **2006**, *369*, 2025–2035. [CrossRef]
42. Stancik, A.L.; Brauns, E.B. A simple asymmetric lineshape for fitting infrared absorption spectra. *Vib. Spectrosc.* **2008**, *47*, 66–69. [CrossRef]
43. Hadj Larbi, F.; Khereddine, A.; Alili, B.; Bradai, D. Généralisation des expressions analytiques liées à la fonction pseudo-Voigt utilisée en analyse des profils de raies de diffraction. *Fizika A* **2009**, *18*, 63–72.
44. Wertheim, G.K.; Butler, M.A.; West, K.W.; Buchanan, D.N. Determination of the Gaussian and Lorentzian content of experimental line shapes. *Rev. Sci. Instrum.* **1974**, *45*, 1369–1371. [CrossRef]

45. Sánchez-Bajo, F.; Cumbrera, F.L. The use of the pseudo-Voigt function in the variance method of X-ray line-broadening analysis. *J. Appl. Crystallogr.* **1997**, 30, 427–430. [CrossRef]
46. Liu, Y.; Lin, J.; Huang, G.; Guo, Y.; Duan, C. Simple empirical analytical approximation to the Voigt profile. *JOSA B* **2001**, *18*, 666–672. [CrossRef]
47. Di Rocco, H.O.; Cruzado, A. The Voigt profile as a sum of a Gaussian and a Lorentzian functions, when the weight coefficient depends only on the widths ratio. *Acta Phys. Pol. A* **2012**, *122*, 666–669. [CrossRef]
48. Ida, T.; Ando, M.; Toraya, H. Extended pseudo-Voigt function for approximating the Voigt profile. *J. Appl. Crystallogr.* **2000**, *33*, 1311–1316. [CrossRef]
49. Thompson, P.; Cox, D.E.; Hastings, J.B. Rietveld refinement of Debye-Scherrer synchrotron X-ray data from Al_2O_3. *J. Appl. Crystallogr.* **1987**, *20*, 79–83. [CrossRef]
50. Whiting, E.E. An empirical approximation to the Voigt profile. *J. Quant. Spectrosc. Radiat. Transf.* **1968**, *8*, 1379–1384. [CrossRef]
51. Olivero, J.J.; Longbothum, R.L. Empirical fits to the Voigt line width: A brief review. *J. Quant. Spectrosc. Radiat. Transf.* **1977**, *17*, 233–236. [CrossRef]
52. Kielkopf, J.F. New approximation to the Voigt function with applications to spectral-line profile analysis. *JOSA* **1973**, *63*, 987–995. [CrossRef]
53. Dobrichev, V. A simple one per cent approximation of the Voigt function. *CR Acad. Bulg. Sci.* **1984**, *37*, 991–993.
54. He, J.; Zhang, Q. An exact calculation of the Voigt spectral line profile in spectroscopy. *J. Opt. A Pure Appl. Opt.* **2007**, *9*, 565–568. [CrossRef]
55. He, J.; Zhang, Q. Discussion on the full width at half maximum (FWHM) of the Voigt spectral line. *Optik* **2013**, *124*, 5245–5247. [CrossRef]
56. He, J.; Zhang, C. The accurate calculation of the Fourier transform of the pure Voigt function. *J. Opt. A Pure Appl. Opt.* **2005**, *7*, 613–616. [CrossRef]
57. Wang, Y.; Zhou, B.; Zhao, R.; Wang, B.; Liu, Q.; Dai, M. Super-accuracy calculation for the half width of a Voigt profile. *Mathematics* **2022**, *10*, 210. [CrossRef]
58. Karp, A.H. Efficient computation of spectral line shapes. *J. Quant. Spectrosc. Radiat. Transf.* **1978**, *20*, 379–384. [CrossRef]
59. Reiche, F. Über die Emission, Absorption und Intensitätsverteilung von Spektrallinien. *Ber. Deutsch. Phys. Ges.* **1913**, *15*, 3–21.
60. Mitchell, A.C.G.; Zemansky, N.W. *Resonance Radiation and Excited Atoms*; Cambridge University Press: Cambridge, UK, 1934; p. 319.
61. Lambert, J.H. Observationes Variae in Mathesin Puram. *Acta Helv. Phys.-Math.-Anat.-Bot.-Med.* **1758**, *3*, 128–168.
62. Lambert, J.H. *Nouveaux Mémoires de l'Académie Royale des Sciences et Belles-Lettres de Berlin*; German Academy of Sciences Berlin: Berlin, Germany, 1772.
63. Corless, R.M.; Gonnet, G.H.; Hare, D.E.G.; Jeffrey, D.J.; Knuth, D.E. On the Lambert *W* function. *Adv. Comput. Math.* **1996**, *5*, 329–359. [CrossRef]
64. Dubinova, I.D. Application of the Lambert *W* function in mathematical problems of plasma physics. *Plasma Phys. Rep.* **2004**, *30*, 937–943. [CrossRef]
65. Valluri, S.R.; Gil, M.; Jeffrey, D.J.; Basu, S. The Lambert *W* function in quantum statistics. *J. Math. Phys.* **2009**, *50*, 102103. [CrossRef]
66. Wilson, B.G.; Sonnad, V. A note on generalized radial mesh generation for plasma electronic structure. *High Energy Density Phys.* **2011**, *7*, 161–162. [CrossRef]
67. Pain, J.-C. Comment on "A note on generalized radial mesh generation for plasma electronic structure". *High Energy Density Phys.* **2011**, *7*, 224. [CrossRef]
68. Bowen, C.; Pain, J.-C. Schrödinger equation on a generic radial grid. *High Energy Density Phys.* **2023**, *47*, 101042. [CrossRef]
69. Visser, M. Primes and the Lambert *W* function. *Mathematics* **2018**, *6*, 56. [CrossRef]
70. Euler, L. De serie Lambertina Plurimisque eius insignibus proprietatibus. *Acta Acad. Sci. Imp. Petropolitanae* **1783**, *2*, 29–51.
71. Comtet, L. Inversion de $y^\alpha e^y$ et $y \log^\alpha y$ au moyen des nombres de Stirling. *CR Acad. Sci. Paris* **1970**, *270*, 1085–1088.
72. Jeffrey, D.J; Corless, R.M.; Hare, D.E.G.; Knuth, D.E. Sur l'inversion de $y^\alpha e^y$ au moyen des nombres de Stirling associés. *CR Acad. Sci. Paris* **1995**, *320*, 1449–1452.
73. Hassani, M. Approximation of the Lambert W Function. *Rgmia Res. Rep. Collect.* **2005**, *8*, 12.
74. Comtet, L. *Advanced Combinatorics*; D. Reidel Publishing Company: Dordrecht, The Netherlands, 1974.
75. Mitrinović, D.S.; Doković, D. Sur une relation de récurrence concernant les nombres de Stirling. *CR Acad. Sci.* **1960**, *250*, 2110–2111.
76. Karanicoloff, C. Sur une représentation des nombres de Stirling dans une forme explicite. *Publ. Elektrotehničkog Fak. Ser. Mat. Fiz.* **1961**, *67*, 9–10. (In French)
77. Graham, R.L.; Knuth, D.E.; Patashnik, O. *Concrete Mathematics*; Addison-Wesley: Boston, MA, USA, 1994.
78. Iglesias, C.A.; Sonnad, V.; Wilson, B.G.; Castor, J.I. Frequency dependent electron collisional widths for opacity calculations. *High Energy Density Phys.* **2009**, *5*, 97–104. [CrossRef]
79. Dufty, J.W. Charge-density fluctuations in spectral line broadening. *Phys. Rev.* **1969**, *187*, 305–313. [CrossRef]
80. Dufty, J.W. Ion motion in plasma line broadening. *Phys. Rev. A* **1970**, *2*, 534–541. [CrossRef]
81. Lee, R.W. *Spectral Line-Broadening Codes for Hydrogen-, Helium- and Lithium-like Ions in Plasmas*; LLNL-Report, UCID-21292; NASA/ADS: Cambridge, MA, USA, 1987.

82. Lee, R.W. Plasma line shapes for selected transitions in hydrogen-, helium- and lithium-like ions. *J. Quant. Spectrosc. Radiat. Transf.* **1988**, *40*, 561–568. [CrossRef]
83. Cowley, E.R.; Zekaria, F. Moment-expansion-method calculations of phonon line shapes in argon. *Phys. Rev. B* **1994**, *50*, 16380–16385. [CrossRef] [PubMed]
84. Viswanath, V.S.; Zhang, S.; Stolze, J.; Muller, G. Ordering and fluctuations in the ground state of the one-dimensional and two-dimensional S = 1/2 − *XXZ* antiferromagnets: A study of dynamical properties based on the recursion method. *Phys. Rev. B* **1994**, *49*, 9702–9715. [CrossRef]
85. Blumstein, C.; Wheeler, C. Modified-moments method: Applications to harmonic solids. *Phys. Rev. B* **1973**, *8*, 1764–1776. [CrossRef]
86. Michette, A.G.; Pfauntsch, S.J. Laser plasma X-ray line spectra fitted using the Pearson VII function. *J. Phys. D Appl. Phys.* **2000**, *33*, 1186–1190. [CrossRef]
87. Wang, H.; Zhou, J. Numerical conversion between the Pearson VII and pseudo-Voigt functions. *J. Appl. Cryst.* **2005**, *38*, 830–832. [CrossRef]
88. Sapar, A.; Poolamäe, R.; Sapar, L. High-precision approximation expressions for line profiles of hydrogenic particles. *Balt. Astron.* **2006**, *15*, 435-447.
89. Pain, J.-C. Expression of the Holtsmark function in terms of hypergeometric ${}_2F_2$ and Airy Bi functions. *Eur. Phys. J. Plus* **2020**, *135*, 236. [CrossRef]
90. Fried, B.D.; Conte, S.D. *The Plasma Dispersion Function*; Academic Press: New York, NY, USA; London, UK, 1961.
91. Drayson, S.R. Rapid computation of the Voigt profile. *J. Quant. Spectrosc. Radiat. Transf.* **1976**, *16*, 611–614. [CrossRef]
92. Dawson, J.; Obermann, C. High-frequency conductivity and the emission and absorption coefficients of a fully ionized plasma. *Phys. Fluids* **1962**, *5*, 517–524. [CrossRef]
93. Kim, T.-S.; Carswell, R.F.; Cristiani, S.; D'Odorico, S.; Giallongo, E. The physical properties of the Lyα forest at $z > 1.5$. *Mon. Not. R. Astron. Soc.* **2002**, *335*, 555–573. [CrossRef]
94. Mihalas, D. *Stellar Atmospheres*; W. H. Freeman and Company: New York, NY, USA, 1971.
95. Harris, D.L., III. On the line-absorption coefficient due to Doppler effect and damping. *Astrophys. J.* **1948**, *108*, 112–115. [CrossRef]